NeuroImage: Clinical 22 (2019) 101777

Contents lists available at ScienceDirect

NeuroImage: Clinical

journal homepage: www.elsevier.com/locate/ynicl

Mechanisms of functional compensation, delineated by eigenvector centrality mapping, across the pathophysiological continuum of Alzheimer's disease

Stavros Skouras[a], Carles Falcon[a,b], Alan Tucholka[a], Lorena Rami[c], Raquel Sanchez-Valle[c], Albert Lladó[c], Juan D. Gispert[a,b], José Luís Molinuevo[a,c,*]

[a] Barcelonaβeta Brain Research Center (BBRC), Pasqual Maragall Foundation, Barcelona, Spain
[b] Biomateriales y Nanomedicina (CIBER-BBN), Centro de Investigación Biomédica en Red de Bioingeniería, Madrid, Spain
[c] Alzheimer's Disease and Other Cognitive Disorders Unit, Hospital Clínic, Institut d'Investigacions Biomèdiques August Pi i Sunyer (IDIBAPS), Barcelona, Spain

ARTICLE INFO

Keywords:
Resting-state fMRI
Eigenvector centrality
Functional connectomics
Hippocampus
Neural capacity

ABSTRACT

Background: Mechanisms of functional compensation throughout the progression of Alzheimer's disease (AD) remain largely underspecified. By investigating functional connectomics in relation to cerebrospinal fluid (CSF) biomarkers across the pathophysiological continuum of AD, we identify disease-stage-specific patterns of functional degradation and functional compensation.

Methods: Data from a sample of 96 participants, comprised of 49 controls, 11 preclinical AD subjects, 21 patients with mild cognitive impairment (MCI) due to AD and 15 patients with mild dementia due to AD, were analyzed. CSF ratio of phosphorylated tau protein over amyloid beta peptide 42 (p-tau/Aβ42) was computed and used as a marker of progression along the AD continuum. Whole-brain, voxel-wise eigenvector centrality mapping (ECM) was computed from resting-state fMRI and regression against p-tau/Aβ42 was performed. Surviving clusters were used as data-derived seeds in functional connectivity analyses and investigated in relation to memory performance scores (delayed free recall and memory alteration) via complementary regression models. To investigate disease-stage-specific effects, the whole-brain connectivity maps of each cluster were compared between progressive groups.

Results: Centrality in BA39-BA19 is negatively correlated with the p-tau/Aβ42 ratio and associated to memory function impairment across the AD continuum. The thalamus, anterior cingulate (ACC), midcingulate (MCC) and posterior cingulate cortex (PCC) show the opposite effect. The MCC shows the highest increase in centrality as memory performance decays. In the asymptomatic preclinical group, MCC shows reduced functional connectivity (FC) with the left hippocampus and stronger FC with the precuneus (PCu). Additionally, BA39-BA19 show reduced FC with the cerebellum, compensated by stronger FC between cerebellum and PCC. In the MCI group, PCC shows reduced FC with PCu, compensated by stronger FC with the left pars orbitalis, insula and temporal pole, as well as by stronger FC of MCC with its anterior and ventral neighboring areas and the cerebellum. In the mild dementia group, extensive functional decoupling occurs across the entire autobiographical memory network and functional resilience ensues in posterior regions and the cerebellum.

Conclusions: Functional decoupling in preclinical AD occurs predominantly in AD-vulnerable regions (e.g. hippocampus, cerebellar lobule VI / Crus I, visual cortex, frontal pole) and coupling between MCC and PCu, as well as between PCC and cerebellum, emerge as intrinsic mechanisms of functional compensation. At the MCI stage, the PCu can no longer compensate for hippocampal decoupling, but the compensatory role of the MCC and PCC ensue into the stage of dementia. These findings shed light on the neural mechanisms of functional compensation across the pathophysiological continuum of AD, highlighting the compensatory roles of several key brain areas.

Abbreviations: Aβ42, amyloid beta peptide 42; ACC, Anterior Cingulate Cortex; AD, Alzheimer's disease; BA, Brodmann Area; CSF, Cerebrospinal Fluid; EC, Eigenvector Centrality; ECM, Eigenvector Centrality Mapping; FC, Functional Connectivity; IPL, Inferior Parietal Lobule; MCC, Middle Cingulate Cortex; MCI, Mild Cognitive Impairment; PCC, Posterior Cingulate Cortex; PCu, Precuneus; P-tau, phosphorylated tau protein.

* Corresponding author at: Barcelonaβeta Brain Research Center, C/ Wellington 30, Barcelona E-08005, Spain.
E-mail address: jlmolinuevo@barcelonabeta.org (J.L. Molinuevo).

https://doi.org/10.1016/j.nicl.2019.101777
Received 8 June 2018; Received in revised form 8 February 2019; Accepted 10 March 2019
Available online 12 March 2019

1. Introduction

AD is a devastating neurodegenerative disease bolstered by a complex mechanism that has remained the subject of investigations for over a century since its initial characterization (Strassnig and Ganguli, 2005). During a tacit process of disease incubation that can last several decades, the disease remains asymptomatic. Once symptoms such as episodic memory decline, cognitive impairment and neurodegeneration become apparent, the disease is already in an advanced stage (Sperling et al., 2011). Subjects at the early stages of the pathophysiological continuum of AD maintain neuropsychological performance that is indistinguishable from healthy participants on the individual level (Dubois et al., 2016). Due to this reason, preclinical AD offers a unique window into mechanisms of functional compensation that enable the brain to exhibit resilience, reorganize adaptively and maintain unaffected functionality under the pressure of biological changes that eventually lead to neurodegeneration. FMRI methods are beginning to distinguish subtle functional changes that precede irreversible neurodegeneration (Sheline and Raichle, 2013; Leal et al., 2017; Palmqvist et al., 2017) while the brain remains able to compensate functional changes robustly (Pihlajamäki and Sperling, 2008; Teipel et al., 2015).

The cerebrospinal fluid (CSF) ratio of phosphorylated tau protein to amyloid beta peptide 42 (p-tau/Aβ42) has been used as a marker of individual pathophysiology alterations along the continuum from normal cognition to dementia due to AD (Maddalena et al., 2003). The p-tau/Aβ42 ratio has scored well as a predictor of cognitive decline in non-demented older adults (Fagan et al., 2007) and has been comparatively assessed with regards to diagnostic power across different populations (Molinuevo et al., 2013). Evidence suggested the p-tau/Aβ42 ratio as the most effective biomarker index for distinguishing dementia due to AD from semantic and frontotemporal dementias (de Souza et al., 2011). Effects of amyloid beta levels on resting state functional connectivity (FC) have recently been investigated in cognitively normal subjects (Elman et al., 2016; Palmqvist et al., 2017), suggesting effects on the intra-network and inter-network connectivity of the default mode network (DMN). In contrast to biomarkers based on measurements of only amyloid or only tau, the p-tau/Aβ42 ratio increases without saturating across the pathophysiological continuum of AD (Li et al., 2007). Thus, using the p-tau/Aβ42 ratio as a regressor of interest, enables addressing incremental and progressive connectomic changes along the entire continuum of AD, including healthy controls and the evasive preclinical phase.

Contemporary theories of network-based degradation and compensation propose that in the face of neurological insult, brain network nodes with low neural reserve degrade first while nodes with high neural reserve perform a compensatory role (Reuter-Lorenz and Cappell, 2008; Seeley et al., 2009; Barulli and Stern, 2013; Jacobs et al., 2013). Recent evidence shows that early β-amyloid accumulation occurs predominantly in the DMN, concurrently affecting functional connectivity in an inverted u-shaped manner, centered around the threshold of amyloid positivity (Palmqvist et al., 2017). This is consistent with previous accounts of an initial increase of posterior DMN connectivity in the preclinical stage of AD, followed by a decrease of DMN connectivity in AD patients (Jack et al., 2013a; 2013b). The DMN is not only associated to task-induced deactivations (Gusnard and Raichle, 2001), but it is also related to attending to the external environment (Shulman et al., 1997; Raichle et al., 2001; Gilbert et al., 2007) as well as to episodic and autobiographical memory (Andrews-Hanna et al., 2010), some of the primary functions afflicted by AD. In this context, the increased functional connectivity observed in the asymptomatic stages of the pathophysiological continuum of AD, appears to reflect processes of functional compensation.

Eigenvector centrality mapping (ECM) is an assumption-free, data-driven procedure that can be performed to identify network nodes acting as hubs of connectivity and influence (Lohmann et al., 2010; Wink et al., 2012). ECM can use the timeseries from all voxels to compute the eigenvector centrality (EC) of each voxel and can be particularly useful in uncovering small-world networks via functional connectivity (Koelsch and Skouras, 2014; Schoonheim et al., 2014). A previous study has shown that ECM of rs-fMRI in AD patients reveals similar patterns as FDG-PET, although less pronounced, across brain lobes (Adriaanse et al., 2016). Another pioneering study investigated changes of rs-fMRI in AD patients using voxel-wise ECM (Binnewijzend et al., 2014). In that study, EC during rs-fMRI was compared in AD patients versus their healthy family members and group differences of EC were observed in the anterior cingulate cortex (ACC) and cuneus. To our knowledge, the present study is the first to investigate resting-state EC in AD with voxel-wise resolution at 3 Tesla. Therefore, compared to previous ECM studies in AD, the present study features increased sensitivity in small subcortical areas that are of particular interest in AD, due to increased magnetic field strength (Skouras et al., 2014), as well as due to voxel-wise resolution. Moreover, our study is one of the first fMRI studies to use biomarkers for AD staging, in accordance with recent research guidelines (Jack et al., 2018), as well as a spatial normalization procedure that is appropriate for including both healthy and neurodegenerated brains into the same analysis (Avants et al., 2008; Avants et al., 2010a). Importantly, this is the first functional neuroimaging study to use a data-driven method for the derivation of seeds used in functional connectivity (FC) comparisons across multiple, consecutive disease stages and the first study of ECM in AD that includes the cerebellum in its field of view.

By pairing the specificity of the p-tau/Aβ42 CSF biomarker with ECM, complemented by advanced normalization techniques to control for differences in brain morphology, we identify brain regions that become incrementally less central as the disease progresses and regions that concurrently compensate by becoming more central. Further testing confirms that centrality changes in these regions are implicated in memory function and the regions are used as seeds to investigate the underlying, intrinsic, progressive changes in FC that occur in each specific stage of AD. Due to its involvement in memory loss and neurodegeneration, the hippocampus and other previously established AD-vulnerable areas, e.g. inferior parietal lobule (IPL), angular gyrus, precuneus (PCu) and visual cortex (Dickerson et al., 2009) were hypothesized to be decreasing in centrality along the AD continuum, whereas the ACC and cuneus were hypothesized to be increasing (Binnewijzend et al., 2014). We expected that clusters which were decreasing in EC across the AD continuum would be decreasing FC with the rest of the brain (e.g. Sheline and Raichle, 2013; Jack et al., 2013a; Jacobs et al., 2013) and we were particularly interested in the temporal evolution of these decreases. Excluding most areas belonging to the DMN, for which we also expected to observe FC decreases (Palmqvist et al., 2017), we expected that clusters increasing in EC would be increasing FC with the same regions that became decoupled from clusters that were decreasing in EC, especially during the preclinical and MCI stages. Finally, with regards to the PCC/PCu in particular, we expected to observe increased FC in the preclinical stage and decreased FC in the rest of the pathophysiological continuum of AD (Jack et al., 2013b).

2. Material and methods

2.1. Subjects

A total of 96 subjects participated in the study, at the 'AD and other cognitive disorders unit', Hospital Clinic i Universitari, (Barcelona, Spain): 49 controls, 11 preclinical AD subjects, 21 patients with mild cognitive impairment due to AD (MCI) and 15 patients with mild dementia due to AD. The study was approved by the local ethics committee and informed consent was obtained from all participants and caregivers in accordance with the Declaration of Helsinki. A larger number of subjects had undergone clinical and neuropsychological assessment, lumbar puncture (LP), MRI scanning, and CSF analysis. Final inclusion eligibility was determined based on: a) completeness of data

(anatomical T1 data, rs-fMRI data, CSF p-tau and Aβ42 values, Apolipoprotein E genotype, neuropsychological tests and demographics); b) unambiguous diagnosis by two neurologists and one neuropsychologist; c) no comorbid clinical pathology; d) no excessive movement during functional neuroimaging.

Categorization into groups was based on the following criteria: a) Controls were CSF Aβ42 negative (over 550 pg/mL) and presented no evidence of cognitive impairment on any of the administered neuropsychological tests, in accordance with the National Institute on Aging-Alzheimer's Association (NIA-AA) criteria (Sperling et al., 2011); b) Preclinical AD subjects presented no evidence of cognitive impairment and were CSF Aβ42 positive; c) Subjects of the MCI group were CSF Aβ42 positive and featured preserved functionality regarding daily activities. After accounting for the effects of age and education, MCI subjects scored below 6 on the Functional Activities Questionnaire and they also scored below 1.5 standard deviations from the sample mean on the total recall measure of the Free and Cued Selective Reminding Test (FCSRT; Grober et al., 2009) as well as on at least one other cognitive test (supplementary table 1). d) Subjects of the dementia due to AD group, fulfilled the NIA-AA criteria for dementia due to AD, were CSF Aβ42 positive and in the mild stages of the disease, i.e. a score of 4 on the Global Deterioration Scale (Wesson and Luchins, 1992) (Table 1).

2.2. CSF sampling and calculation of the CSF biomarker index

All subjects underwent lumbar puncture during standard morning hours (9:00–12:00 AM). Polypropylene tubes were used to sample ten milliliters of CSF from each subject. Samples were centrifuged and stored at −80 °C within one hour from collection. Using enzyme-linked immunosorbent assay kits (Furirebio-Europe, previously known as Innogenetics, Ghent, Belgium), levels of amyloid peptide Aβ42 and phosphorylated tau (p-tau) were measured. The p-tau/Aβ42 ratio, was calculated for each subject, as previously described (Maddalena et al., 2003).

2.3. Image acquisition

All subjects underwent MRI scanning on a 3 T MRI scanner (Magnetom Trio Tim, Siemens, Erlangen, Germany). Each scanning session comprised of one high-resolution three-dimensional structural T1-weighted image acquisition (MPRAGE; TR = 2300 ms, TE = 2.98 ms, matrix size = 256 × 256, 240 sagittal slices, voxel size = 1 × 1 × 1 mm^3) and one ten-minute resting state fMRI acquisition (300 volumes, TR = 2000 ms, TE = 16 ms, matrix size = 128 × 128, 40 axial slices, voxel size = 1.72 × 1.72 × 3 mm^3, interslice gap = 0.75 mm). Subjects were instructed to remain still with their eyes open.

2.4. Image processing and analysis

To enable maximal cortical segmentation accuracy, T1 images were subjected to the N4 nonparametric nonuniform intensity normalization bias correction function (Tustison et al., 2010, 2013) of the Advanced Normalization Tools (ANTs; version 2.x, committed in January 2016; http://stnava.github.io/ANTs/;Avants et al., 2009) and to an optimized blockwise non-local means denoising filter (Coupé et al., 2008). VBM8 (Structural Brain Mapping Group, University of Jena, Jena, Germany; http://www.neuro.uni-jena.de/vbm/) and SPM12 (Wellcome Department of Imaging Neuroscience Group, London, UK; http://www.fil.ion.ucl.ac.uk/spm) were used to segment each subject's anatomical image into grey matter, white matter and CSF. Whole-brain images with removed cranium were also derived through graph-cut (Sadananthan et al., 2010) and FSL (Analysis Group, FMRIB, Oxford, UK; https://fsl.fmrib.ox.ac.uk/fsl/) and used to compute the optimal custom anatomical template for our sample, via the ANTs multivariate template construction procedure (Avants, Tustison et al., 2010; Avants et al., 2010b) that provides optimal results in datasets with neurodegeneration (Avants et al., 2008; Avants et al., 2010a). Using SyGN, neuroanatomically plausible symmetric diffeomorphic matrices were computed to transform each subject's anatomical data to the optimal template and subsequently to MNI space (Avants, Tustison et al., 2010; Tustison and Avants, 2013) as defined by the ICBM brain featuring high signal-to-noise ratio, sharp resolution and detailed gyrification while minimizing biases due to abnormal anatomy (Fonov et al., 2011). The cranium of the ICBM template had also been removed, similarly as for the anatomical data, prior to the normalization of datasets.

Using Matlab 2014b (MathWorks Inc. Natick, MA) and SPM12, functional data were subjected to a typical rs-fMRI preprocessing pipeline comprised of slicetime correction, estimation of movement

Table 1
Demographics and background data.

	Control $n_a = 49$	Preclinical AD $n_b = 11$	MCI due to AD $n_c = 21$	AD dementia $n_d = 15$	Group effect
p-tau/Aβ42	M = 0.067 SD = 0.02	M = 0.158 SD = 0.09	M = 0.374 SD = 0.17	M = 0.382 SD = 0.20	F(3,92) = 49.910 $P < 0.001$
Delayed free recall	M = 10.729 SD = 1.96	M = 8.909 SD = 3.11	M = 2.5 SD = 3.26	M = 2 SD = 2.33	F(3,92) = 81.260 P < 0.001
Memory alteration	M = 46.290 SD = 2.89	M = 43.91 SD = 4.13	M = 32.24 SD = 6.11	M = 27.5 SD = 7.75	F(3,92) = 81.179 P < 0.001
Age	M = 59.816 SD = 6.62	M = 68 SD = 7.11	M = 69.571 SD = 7.92	M = 65.667 SD = 9.95	F(3,92) = 10.068 P < 0.001
p-tau	M = 49.897 SD = 12.25	M = 56.299 SD = 26.78	M = 120.29 SD = 39.67	M = 112.496 SD = 52.87	F(3,92) = 35.673 P < 0.001
Aβ42	M = 758.111 SD = 91.54	M = 381.458 SD = 92.07	M = 341.79 SD = 79	M = 312.069 SD = 86.04	F(3,92) = 179.707 P < 0.001
Education	M = 3.082 SD = 0.84	M = 2.727 SD = 0.79	M = 2.476 SD = 1.12	M = 2.467 SD = 1.25	F(3,92) = 2.750 P < 0.05
Sex ratio (M / F)	17 / 32	3 / 8	9 / 12	7 / 8	$X^2(3, N = 96) = 14.14$ $P = 0.694$
ApoE4 carriers	12%	45%	57%	53%	$X^2(3, N = 96) = 14.14$ P < 0.001

The participants' groups have differed in terms of the relative prevalence of ApoE4 carriers. However, the differences are taken to reflect the actual prevalence of ApoE4 in Alzheimer's disease. Due to the small number of ApoE4 carriers in our sample, including this information in the statistical models would not produce more reliable findings. Due to regional differences and historical changes in the educational system, education was modeled as an ordinal variable with a coding of "0" corresponding to no education, "1" corresponding to elementary school education, "2" corresponding to middle school education, "3" corresponding to high school education and "4" corresponding to university education.

parameters, coregistration, bandpass filtering between 0.01 and 0.1 Hz and second order detrending to remove slow signal drifts. In all subjects, movement remained below 3 mm for all translation parameters and below 1° for all rotation parameters. For further quality control, the effect of scanning-induced systematic vibration (Gallichan et al., 2010) was investigated by performing Fourier analysis on movement parameters and compensated by use of 'scan nulling' regressors (Lemieux et al., 2007) on affected volumes, i.e. volumes having a correlation coefficient to the mean image of the series that deviated by more than three standard deviations ($r < 0.991$) from the grand mean correlation coefficient for the sample ($r = 0.995$). Average CSF signal, average white-matter signal and 24 Volterra expansion movement parameters were regressed out of each participant's timeseries. The five first and five last fMRI volumes of each series were discarded to avoid artefacts often produced at the edges of timeseries due to preprocessing procedures, resulting in a total of 290 functional volumes for each subject.

Each subject's functional data were masked by the grey matter of their equivalent anatomical datasets using FSL and then normalized to MNI space in accordance with their respective diffeomorphic matrices using ANTs. Using Leipzig Image Processing and Statistical Inference Algorithms (LIPSIA; version 2.2.7 – released in May 2011; Max Planck Institute for Human Cognitive and Brain Sciences, Leipzig, Germany; http://www.cbs.mpg.de/institute/software/lipsia;Lohmann et al., 2000), each functional dataset was smoothed by a 6 mm FWHM kernel and ECM images were computed as previously described (Lohmann et al., 2010), based on positive correlations within each subject's segmented grey matter binary mask. That is, negative correlations were set to 0 and no arbitrary thresholding was applied. In each grey matter voxel, the correlation matrix with all other grey matter voxels was computed and summed to produce the EC value of the first iteration. In following iterations, during the summation of each voxel's correlation matrix, the correlation with each other voxel was weighted by that other voxel's EC value from the previous iteration. In this manner, the EC of each voxel was adjusted iteratively, until further iterations had no effect. With regards to using positive correlations only, it should be noted that EC was initially conceptualized and eventually popularized, due to its success in applications of social network theory and Internet search engines respectively (Bonacich, 1972; Langville and Meyer, 2006), where negative correlations were inexistent or nonsensical. Moreover, current implementations of ECM for neuroimaging, do not yet offer parameter settings for utilizing negative correlations for the computation of the complementary, yet conceptually distinct, beta-centrality (Bonacich, 2007). Alternative parameter settings generate results that are not intuitively interpretable as representing the magnitude of influence that EC is meant to capture (Borgatti, 2005). The "add" method of adding 1 to all correlation coefficients gives an advantage to low negative correlations over high negative correlations, which is meaningful in the context of social cliques (Bonacich and Lloyd, 2004), however not as meaningful in the context of unsegregated whole-brain datasets. Similarly, the "abs" method of using absolute correlations allows both positive and negative correlations to contribute to EC values equally, thereby leading to arbitrarily mixed and potentially uninterpretable results.

2.5. Statistical inference

To enable second-level parametric inference, ECM images were gaussianized voxel-wise across all subjects (Albada and Robinson, 2007). Statistical inference was performed using LIPSIA. Gaussianized ECM images from all subjects were entered into a second-level general linear model (GLM) with p-tau/Aβ42, age, gender, and education as regressors. The effect of p-tau/Aβ42 was computed, producing a z-score contrast image representing the correlations of EC with p-tau/Aβ42 in each grey matter voxel, while accounting for the effects of age, gender and education as covariates of no interest. Clusters with significant correlation between EC and p-tau/Aβ42 were identified following correction for multiple comparisons by using a combination of single-voxel probability thresholding as well as cluster-size and cluster-z-value thresholding, through 1000 iterations of Monte Carlo simulations. The initial naive cluster threshold of randomly generated maps of z-values was set to a probability level equivalent to a two-tail significance level of 0.05, because of the exploratory nature of the regression between p-tau/Aβ42 and EC. The Monte Carlo simulations accounted for anatomical priors through hemispheric symmetry and generated thresholds for cluster sizes and peak z-values given the initial threshold and the specific geometrical properties of the images (i.e. number of voxels, voxel size, spatial extent and spatial smoothness) to control for false positives and obtain the final activation maps corrected for multiple comparisons at the 0.05 level of significance. This was accomplished using the LIPSIA vmulticomp algorithm (Lohmann et al., 2008; Lohmann et al., 2010). Similarly to other state-of-the-art methods for multiple comparisons correction: 1) vmulticomp uses random permutations, robust to assumptions of random field theory (Smith and Nichols, 2009; Cox et al., 2017); 2) vmulticomp produces results that are not dependent on static activation level and spatial extent thresholds (Smith and Nichols, 2009; Cox et al., 2017); 3) vmulticomp separates the statistical modeling step from the permutation-based multiple comparisons correction (Cox et al., 2017). Moreover, according to the recent recommendation of incorporating anatomical information in fMRI statistical inference methods (Brown and Behrmann, 2017), vmulticomp utilizes anatomical priors to mitigate the biases against small anatomical structures and the danger of dismissing strong but spatially small activations often produced by subcortical structures. The algorithm first generates a random noise image via permutations. It then applies to the random image a Gaussian smoothing kernel to make it comparable to data that have been normalized and smoothed during preprocessing. The size of this kernel should not exceed the FWHM smoothness value that was used during preprocessing plus the intrinsic smoothness of the normalized data, which for 3x3x3 isomorphic voxels is equal to 6. The kernel also features a standard deviation derived from the data. Clusters are obtained by applying the naïve cluster threshold to the smoothed random noise image. The algorithm then computes how many clusters would survive by chance, given the specified cluster threshold as well as different triplets of cluster sizes, activation levels and hemispheric symmetry indices. The cluster threshold can be adjusted depending on the effect size under investigation without violating any statistical assumptions, thanks to the robustness of the Monte Carlo framework (Poline et al., 1997). Hemispheric symmetry indices are computed by comparing the degree of co-activation between all voxels in a given cluster and their homotopic voxels in the contralateral hemisphere, by making use of the Talairach stereotactic coordinate system. Clusters characterized by combinations of features that could have been obtained by chance, according to the specified alpha level, are eliminated (Lohmann et al., 2008).

Using a data-driven approach to FC seed derivation, enabled to focus on the progressive FC changes of the brain regions predominantly implicated throughout AD, via an unbiased and information-efficient procedure. Every ECM cluster was used as a seed cluster to calculate its standardized FC, via Fisher's r to z transformation (Fisher, 1915, 1921), with each grey matter voxel across the whole brain of each subject. Second-level GLM design matrices accounting for the effects of age, gender and education as covariates of no interest, were utilized to compute two-sample *t*-tests and discover voxel-wise FC differences of each ECM cluster between: a) control and preclinical groups; b) preclinical and MCI groups; c) MCI and dementia due to AD groups. Clusters featuring significant FC changes with the seed clusters were identified following correction for multiple comparisons, performed identically as for the EC clusters with the exception of setting the initial naive cluster threshold of the randomly generated maps of z-values to a probability level equivalent to a one-tail significance level of 0.05, because of directional hypotheses regarding the FC of ECM clusters and DMN regions. Note that using LIPSIA we computed and corrected for

multiple comparisons a single contrast image for each ECM cluster, that contained both positive and negative z-scores. This approach is more parsimonious than computing positive and negative versions of the same contrast separately, because all positive as well as negative clusters have to compete with each other in terms of size, strength and anatomical plausibility to survive the correction for multiple comparisons (in other software positive clusters only compete with positive and negative only with negative). Moreover, this is what enabled us to test directional hypotheses regarding both positive and negative FC differences, at once.

To investigate whether the primary findings were associated with memory processes, we performed correlation testing between the average ECM of each seed cluster and scores on two important memory tests: delayed free recall score from the FCSRT (Grober and Buschke, 1987) and score on the memory alteration test (M@T; Rami et al., 2007). Because both memory scores showed highly significant correlations with average ECM values in most seed clusters, we repeated the main regression analysis, using identical thresholds but replacing p-tau/Aβ42 by each memory score. We then computed the conjunctions with the p-tau/Aβ42 regression results. The purpose of this process was to precisely assess the specificity of the correlations with the memory performance scores and to identify the memory processes that each seed cluster was most strongly involved in.

3. Results

3.1. Eigenvector centrality across the pathophysiological continuum of AD

An extensive left lateral parieto-occipital ECM cluster, encompassing parts of IPL, posterior Postcentral Gyrus (PGp), BA19 and angular gyrus (BA39), correlated negatively with p-tau/Aβ42 (Table 2; Fig. 1). Concurrently, three distinct clusters that correlated significantly with p-tau/Aβ42 were localized in the cingulate cortex: one in the medial cingulate cortex (MCC), primarily localized at the posterior part of BA24; one in the PCC, primarily localized at the intersection of BA31 and BA23; and one in the ACC, at the intersection between the anterior parts of BA32 and BA24 (Table 2; Fig. 1). An additional cluster in the thalamus, including the ventral anterior nucleus, also correlated positively with p-tau/Aβ42 (Table 2; Fig. 1).

Average EC in all ECM clusters correlated with FCSRT delayed free recall and M@T scores. However, the correlations survived correction for multiple comparisons only in the MCC, thalamus and BA39-BA19 (Table 3). The conjunction between the regression maps for p-tau/Aβ42 and memory scores revealed a significant positive correlation of EC within the BA39-BA19 cluster with FCSRT delayed free recall score and significant negative correlations of EC within the MCC and thalamus clusters with M@T score (Fig. 2).

Table 2
Results of the Eigenvector Centrality Mapping (ECM) correlation with p-tau/Aβ42.

	MNI coord.	Cluster size (mm^3)	z-value: max (mean)
MCC (Area 33)	3 −6 34	567	3.31 (2.42)
PCC	−6 −30 37	540	3.37 (2.41)
L Thalamus (Temporal)	−15 −24 22	1080	3.26 (2.43)
ACC (Area s24/s23)	−6 30 1	864	3.01 (2.27)
L IPL, BA39-BA19 (FG2)	−54 −72 13	3564	−4.13 (−2.73)

Entries in brackets indicate the peak voxel labels with the highest cytoarchitectonic probabilities according to the SPM Anatomy Toolbox (Eickoff et al., 2005). The outermost right column indicates the maximal z-value of voxels within a cluster (with the mean z-value of all voxels within a cluster in parentheses). Abbreviations: MCC: Middle Cingulate Cortex; PCC: Posterior Cingulate Cortex; ACC: Anterior Cingulate Cortex; IPL: Inferior Parietal Lobule.

3.2. Functional connectivity in the preclinical AD group

In the preclinical group, compared to the control group, the ECM cluster in BA39-BA19 showed significantly lower FC with the right postcentral, precentral and supramarginal gyri (including parts of BA2, BA4 and BA3), the right frontal pole, the superior and medial frontal gyrus (primarily BA10) and an occipito-cerebellar cluster including parts of the cuneus, PCu, declive and lingual gyri bilaterally (Table 4; Fig. 3, bottom row). The ECM cluster in MCC showed significantly lower FC with the left hippocampus and concurrently higher FC with the PCu in the preclinical group (Table 4; Fig. 3, top row). The ECM cluster in the PCC showed significantly lower FC with the cerebellum in the preclinical group (Table 4; Fig. 3, second row). The ECM clusters in the ACC and the thalamus did not show any significant differences of FC between the control and the preclinical AD groups.

3.3. Functional connectivity in the MCI due AD group

In the MCI due to AD group, compared to the preclinical AD group, the ECM cluster in the PCC showed significantly lower FC with PCu and concurrently higher FC with the right insula (Table 5; Fig. 4, second row). Additionally, the MCC cluster showed significantly higher FC with the middle part of BA24 and cerebellum in the MCI group (Table 5; Fig. 4, top row). The ECM clusters in BA39-BA19, ACC and the thalamus did not show any significant differences of FC between the preclinical and MCI groups.

3.4. Functional connectivity in the dementia due to AD group

In the dementia due to AD group, compared to the MCI due to AD group, the BA39-BA19 cluster showed significantly lower FC with the middle and superior frontal gyri, including ACC, BA9, BA32, BA10, BA11, as well as the right middle and superior temporal gyri, BA21 and the superior temporal pole (Table 6; Fig. 5, bottom row). Concurrently, significantly higher FC was observed between BA39-BA19 and cerebellum (declive, culmen and vermis lobules VI-VIII).

The MCC cluster showed significantly lower FC with the PCu, posterior cingulate cortex (PCC) and right temporal gyrus in the dementia due to AD group and concurrently increasing FC with the lingual gyri bilaterally (Table 6; Fig. 5, top row). The ACC showed significantly lower FC with the cerebellum, the fusiform gyri bilaterally and the lingual gyri bilaterally in the dementia due to AD group compared to the MCI due to AD group (Table 6; Fig. 5, third row). The PCC cluster showed significantly higher functional connectivity with the PCu, cerebellum and lingual gyri bilaterally in the dementia due to AD group (Table 6; Fig. 5, second row). The ECM cluster in the thalamus did not show any significant differences of FC between the MCI and dementia groups.

4. Discussion

4.1. Eigenvector centrality across the pathophysiological continuum of AD

The extensive left lateral parieto-occipital cluster encompassing BA19 and BA39, that correlated negatively with p-tau/Aβ42, is known to be an area vulnerable to regional cortical thinning in AD (Dickerson et al., 2009; Fortea et al., 2011). A meta-analysis suggests the BA39-BA19 intersection to be important in episodic auto-biographical memory (Martinelli et al., 2013). In healthy young adults, the BA39-BA19 intersection comprises a central part of the cortical hub that features the maximal degree of connectivity with the rest of the brain and is considered to be part of the foremost cortical hub with the highest metabolic demands (Buckner et al., 2009). The observation of a correlation of EC in BA39-BA19 with FCSRT delayed free recall score, suggests the involvement of this region in free recall (Fig. 2). The BA39-BA19 region plays an important role in further memory processes, as

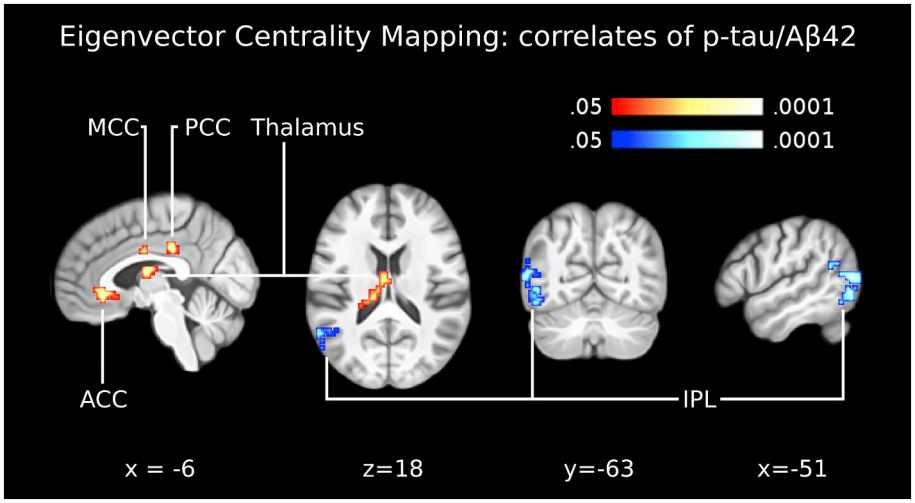

Fig. 1. Eigenvector centrality across the pathophysiological continuum of AD. The panel shows the correlation between eigenvector centrality maps and the CSF biomarker p-tau/Aβ42, across the AD continuum from health to Alzheimer's dementia. Clusters of centrality values significantly correlating positively with p-tau/Aβ42 were indicated in the anterior cingulate cortex (ACC), midcingulate cortex (MCC), posterior cingulate cortex (PCC) and left thalamus. One cluster of centrality values significantly correlating negatively with p-tau/Aβ42 was indicated in the inferior parietal lobule (IPL; BA39-BA19). These five clusters were used as seed regions for functional connectivity analyses (Figs. 2-4). Images are shown in neurological convention; all results are corrected for multiple comparisons ($P < 0.05$). Coordinates refer to MNI space.

Table 3
Correlations between average ECM values in clusters correlating with p-tau/Aβ42 and score on administered memory tests.

	MCC	PCC	Thalamus	ACC	IPL
Delayed free recall	$r = -0.386$ $p < 0.001$	$r = -0.267$ $p = 0.008$	$r = -0.374$ $p < 0.001$	$r = -0.232$ $p = 0.023$	$r = 0.357$ $p < 0.001$
Memory alteration	$r = -0.406$ $p < 0.001$	$r = -0.2748$ $p = 0.007$	$r = -0.394$ $p < 0.001$	$r = -0.233$ $p = 0.022$	$r = 0.392$ $p < 0.001$

Only correlations with $p < 0.001$ remained significant after Bonferroni correction for multiple comparisons.

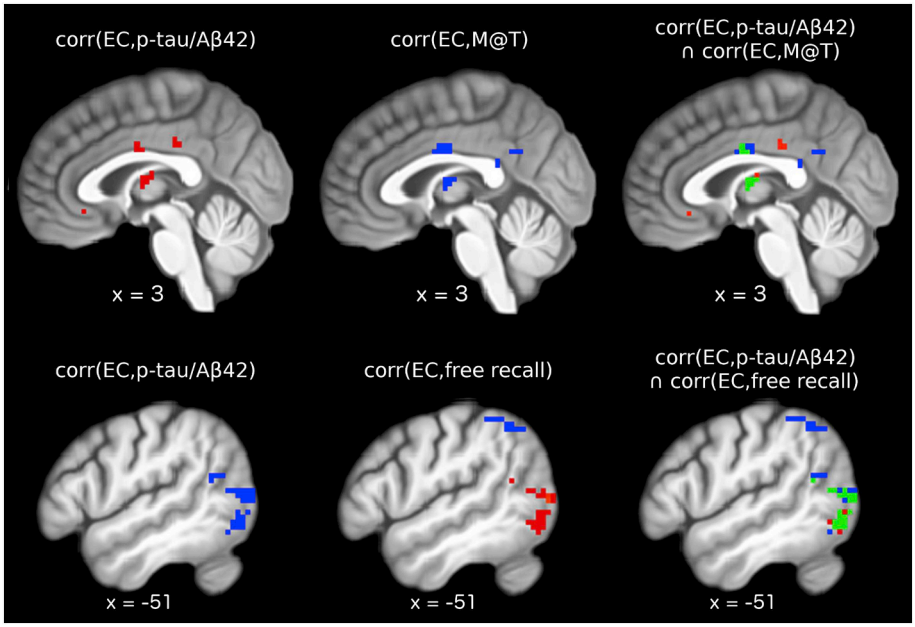

Fig. 2. Conjunction analysis. The main eigenvector centrality regression analysis was repeated twice, replacing p-tau/Aβ42 with score on memory alteration test (M@T) and score on delayed free recall of the free and cued selective reminding test, controlling for age, gender and level of education. Results were corrected for whole-brain multiple comparisons using identical methods to the main analysis. Top row left: significant positive correlations between EC and p-tau/Aβ42; top row middle: significant negative correlations between EC and M@T scores; top row right: green voxels display regions where EC correlated significantly with both p-tau/Aβ42 and M@T scores. Bottom row left: significant negative correlation between EC and p-tau/Aβ42; bottom row middle: significant positive (red) and significant negative (blue) correlations between EC and scores of delayed free recall; bottom row right: green voxels display regions where EC correlated significantly with both p-tau/Aβ42 and delayed free recall scores. (For interpretation of the references to color in this figure legend, the reader is referred to the web version of this article.)

well as in the flexible coupling between the default mode network and the frontoparietal control network subserving autobiographical planning (Spreng et al., 2010). Therefore, given our novel observation of decreasing EC throughout the AD continuum and the lack of cognitive impairment during the preclinical stage of AD that may last up to twenty years (Jack et al., 2018**),** the increasing EC in the cingulate cortex and thalamus presumably represent a compensatory response to the functional degradation of BA39-BA19 and memory performance. This interpretation, is highly plausible because meta-analyses and scientific review articles show: a) the particular parts of MCC (posterior BA24) and ACC (BA32-BA22 intersection) to be involved in working memory (Wager and Smith, 2003); b) the PCC cluster (BA31; BA23) to be involved in self-autobiographical memory (Martinelli et al., 2013); c) the importance of the anterior nucleus of the thalamus in the manifestation of AD (Aggleton et al., 2016).

4.2. Functional connectivity in the preclinical AD group

FC differences of hippocampus and BA24 had previously been observed only between control and MCI groups (Wang et al., 2006). Our results suggest that the onset of the functional decoupling between the hippocampus and BA24 occurs earlier than previously believed, during the preclinical stage. Given no significant alterations in cognitive performance during the preclinical stage (Sperling et al., 2011), the concurrent functional coupling of the exact same BA24 cluster with the PCu emerges as a compensatory mechanism. The PCu, possesses extensive

Table 4
Results of the group-specific functional connectivity analyses for the Preclinical > Control contrast.

	MNI coord.	Cluster size (mm^3)	z-value: max (mean)
(a) MCC (Area 33)			
L Precuneus; L MCC; R PCC	−6 −57 40	3888	3.81 (2.31)
L Hippocampus (CA1–3); HATA; Amygdala	−24 −15 −11	1890	−3.93 (−2.20)
(b) PCC			
R Cerebellar lobule VIIa crus I	27 –69 -14	4806	3.29 (2.12)
L Cerebellar lobule VIIa crus	−30 − 60 -14	2700	3.25 (2.08)
L/R Cerebellar lobule VI; Fusiform Gyrus	-6 -75 -14	1998	3.70 (2.38)
(c) L Thalamus (Temporal)			
n.a.	n.a.	n.a.	n.a.
(d) ACC (Area s24/s23)			
n.a.	n.a.	n.a.	n.a.
(e) L IPL, BA39-BA19 (FG2)			
R PCG (4a/4p/2/3b); SMG (PF/PFt); MFG	48 –15 55	2727	−4.31 (−2.23)
R/L Lingual Gyrus; Calcarine Gyrus; Cerebellum; L Cuneus	−15 -66 19	25,569	−3.90 (−2.26)
R SFG (Fp1); SMG (Fp1/Fp2)	9 69 16	2484	−3.64 (−2.26)

Seed-regions used for the functional connectivity analyses were the data-driven clusters observed in the ECM results (ECM correlation with p-tau/Aβ42). For example, the MCC (which showed a positive correlation between centrality values and p-tau/Aβ42) showed decreased functional connectivity with the left hippocampus and increased functional connectivity with the precuneus in the preclinical group (compared to the control group). Entries in brackets indicate the peak voxel labels with the highest cytoarchitectonic probabilities according to the SPM Anatomy Toolbox (Eickoff et al., 2005). The outermost right column indicates the maximal z-value of voxels within a cluster (with the mean z-value of all voxels within a cluster in parentheses). No significant differences were observed in the thalamus and ACC. Abbreviations: MCC: Middle Cingulate Cortex; PCC: Posterior Cingulate Cortex; ACC: Anterior Cingulate Cortex; IPL: Inferior Parietal Lobule; PCG: Precentral Gyrus; SMG: Supramarginal Gyrus; PCG: Postcentral Gyrus; MFG: Middle Frontal Gyrus; SFG: Superior Frontal Gyrus; SMG: Superior Medial Gyrus; HATA: Hippocampus-Amygdala Transition Area.

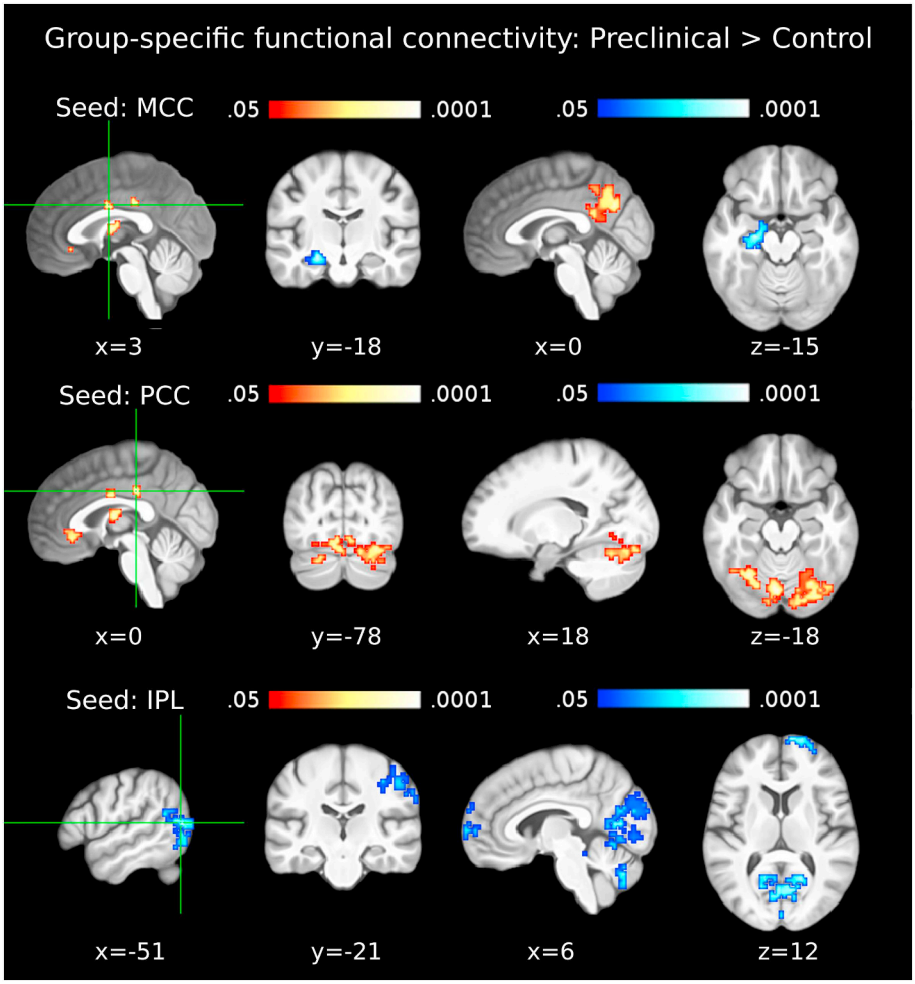

Fig. 3. Functional connectivity in the preclinical AD group. The first column shows seed clusters derived by the data-driven ECM analysis. The results of the comparison of functional connectivity maps between preclinical and control groups (Preclinical > Control) are shown in each row, separately for three seed clusters (MCC: first row, PCC: second row, IPL(BA39-BA19): third row). Each of the two remaining ECM clusters, in the ACC and thalamus, did not show functional connectivity differences between preclinical and control groups. Increases are depicted in red and decreases in blue color; images are shown in neurological convention; all results are corrected for multiple comparisons ($P < 0.05$); coordinates refer to MNI space. (For interpretation of the references to color in this figure legend, the reader is referred to the web version of this article.)

Table 5
Results of the group-specific functional connectivity analyses for the MCI > Preclinical contrast.

	MNI coord.	cluster size (mm^3)	z-value: max (mean)
(a) MCC (Area 33)			
L SMG; MCC; ACC	−6 33 58	2268	3.57 (2.29)
L/R Cerebellar lobule VIIIb[a]	−3 −72 −41	702	4.04 (2.43)
(b) PCC			
L IFG (pars Orbitalis); Insula; STG; Temporal Pole	−36 18 –11	3321	4.24 (2.34)
R/L Calcarine Gyrus (h0c2 - V2); Precuneus	18 –69 22	3294	−2.70 (−2.06)
(c) L Thalamus (Temporal)			
n.a.	n.a.	n.a.	n.a.
(d) ACC (Area s24/s23)			
n.a.	n.a.	n.a.	n.a.
(e) L IPL, BA39-BA19 (FG2)			
n.a.	n.a.	n.a.	n.a.

Seed-regions used for the functional connectivity analyses were the data-driven clusters observed in the ECM results (ECM correlation with p-tau/Aβ42). Entries in brackets indicate the peak voxel labels with the highest cytoarchitectonic probabilities according to the SPM Anatomy Toolbox (Eickoff et al., 2005). The outermost right column indicates the maximal z-value of voxels within a cluster (with the mean z-value of all voxels within a cluster in parentheses). No significant differences were observed in the thalamus, the ACC and BA39-BA19. Abbreviations: MCC: Middle Cingulate Cortex; PCC: Posterior Cingulate Cortex; ACC: Anterior Cingulate Cortex; SMG: Supramarginal Gyrus; IPL: Inferior Parietal Lobule; IFG: Inferior Frontal Gyrus; STG: Superior Temporal Gyrus.

[a] The noted cluster was most extensively localized in Lobule VIIIb, however the peak voxel was localized in left Lobule IX and two further local maxima were observed in right lobule VIIIa and right lobule VIIb

connectivity with several other important brain areas (Cavanna and Trimble, 2006), including the hippocampus, enabling it to compensate hippocampal decoupling from BA24. The meta-analysis of fMRI studies in AD is also aligned with the supposition that the PCu plays a compensatory role during the early stages of the disease, prior to any perceivable cognitive decline (Jacobs et al., 2013). The functional purpose of the increased FC between PCu and BA24, given a functional decoupling between BA24 and hippocampus, could be related to maintaining spatial navigation abilities (Cavanna and Trimble, 2006; Ghaem et al., 1997) and episodic autobiographical memory (Martinelli et al., 2013; Söderlund et al., 2012). With regards to the latter, it is also plausible that the concerned FC increase is further compensating the preclinical decoupling between PCu and BA39-BA19 (Fig. 3; Table 4).

During the preclinical stage, BA39-BA19 decouples not only from the PCu but also from the cuneus, cerebellum, lingual gyri, fusiform gyri, the frontal pole and a cluster containing parts of the right precentral, postcentral and supramarginal gyri. The FC decrease of BA39-BA19 with the cerebellum, lingual gyri and fusiform gyri is compensated by FC increases of PCC with the cerebellum, lingual gyri and fusiform gyri (Fig. 3; Table 4). However, the FC decrease of BA39-BA19 with the part of the occipital cluster localized in the primary and secondary visual cortices remains uncompensated. Our findings suggest that the FC decrease of BA39-BA19 with the visual cortex is prolonged through the subsequent stages of AD, plausibly relating to AD-characteristic regional cortical thinning of both the IPL and the visual cortex (Dickerson et al., 2009). Further areas with early uncompensated FC decreases are the right lateral cluster spreading between the postcentral, precentral and supramarginal gyri and the cluster located in the frontal pole. Collectively, the uncompensated decreases of FC in the preclinical stage correspond to the neural correlates of subtle cognitive effects accounting for changes in global cognitive ability (Bäckman et al., 2005).

To our knowledge, this is the first evidence of cerebellar FC changes occurring in the preclinical stage of AD. Similar cerebellar subregions to the ones identified in our study, specifically Crus I/II and lobule VI, are targeted by atrophy in AD and frontotemporal dementia, respectively (Guo et al., 2016). Although the exact details of these patterns remain to be clarified, current evidence suggest FC of Crus I/II predominantly with the executive network and of lobule VI with the salience network (Habas et al., 2009; Skouras et al., 2018). Additionally, both cerebellar regions have been found to correlate with the anterior prefrontal cortex. In the present study, noticeable overlap between the clusters shown in Fig. 3 (second row and third row) was observed in lobule VI/Crus I (supplementary fig. S1). Given no noticeable cognitive impairment in the preclinical stage, our observation supports the idea that the

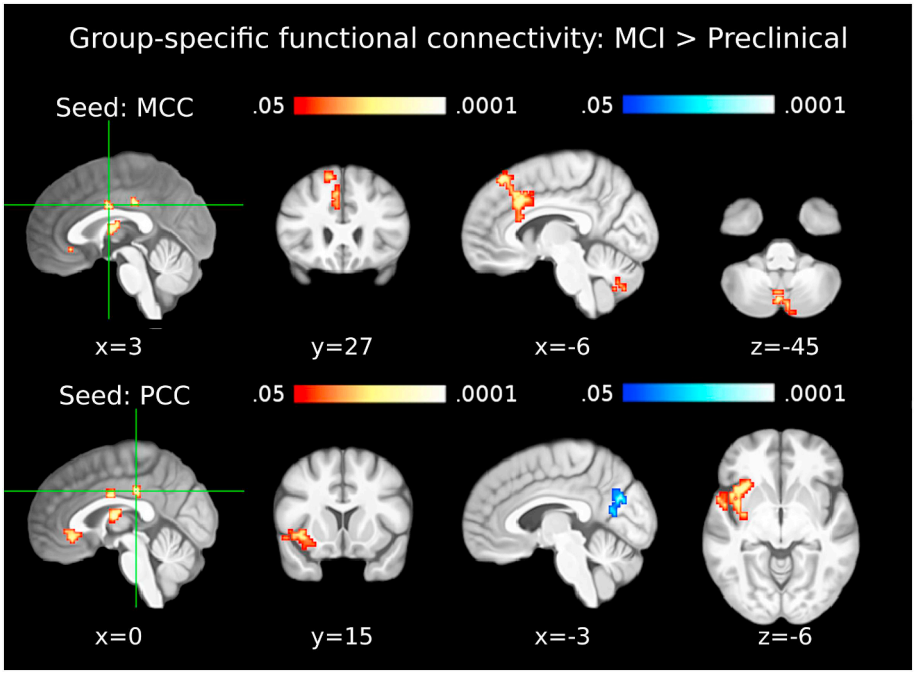

Fig. 4. Functional connectivity in the MCI due to AD group. The first column shows seed clusters derived by the data-driven ECM analysis. The results of the comparison of functional connectivity maps between mild cognitive impairment (MCI) and preclinical groups (MCI > Preclinical) are shown in each row, separately for two seed regions (MCC: first row, PCC: second row). Each of the three remaining ECM clusters, in the ACC, thalamus and IPL (BA39-BA19), did not show functional connectivity differences between MCI and preclinical groups. Increases are depicted in red and decreases in blue color; images are shown in neurological convention; all results are corrected for multiple comparisons ($P < 0.05$); coordinates refer to MNI space. (For interpretation of the references to color in this figure legend, the reader is referred to the web version of this article.)

Table 6
Results of the group-specific functional connectivity analyses for the Dementia > MCI contrast.

	MNI coord.	cluster size (mm^3)	z-value: max (mean)
(a) MCC (Area 33)			
R/L Cerebellar lobule VI	0 −78 4	1728	3.52 (2.40)
L PCC	−3 −48 37	2376	−3.44 (−2.17)
R MTG	60 −33 1	1242	−4.16 (−2.51)
(b) PCC			
L Cerebellar lobules V-VI; Calcarine Gyrus; Cuneus; R Precuneus[a]	−6 −66 −5	14,823	3.68 (2.19)
(c) L Thalamus (Temporal)			
n.a.	n.a.	n.a.	n.a.
(d) ACC (Area s24/s23)			
L Cerebellar lobules VI-VIIa crus I; Fusiform Gyrus; Lingual Gyrus	−27 −60 −2	3213	−4.44 (−2.0
R Cerebellar lobules V-VIIa crus I; Fusiform Gyrus; Lingual Gyrus	33 –63 −14	2349	−3.02 (−2.12)
(e) L IPL, BA39-BA19 (FG2)			
L/R Cerebellar lobule VIIIa, VIIb[b]	−3 –66 −23	1134	3.66 (2.31)
L Rectal Gyrus (Fo1); SMG; ACC	−6 42 25	2106	−2.75 (−2.05)
R Rectal Gyrus (Fp2/Fo1); ACC (s32)	9 69 1	11,313	−3.85 (−2.06)
R Temporal Pole; STG; MTG	51 0 –2	2700	−3.57 (−2.21)

Seed-regions used for the functional connectivity analyses were the data-driven clusters observed in the ECM results (ECM correlation with p-tau/Aβ42). Entries in brackets indicate the peak voxel labels with the highest cytoarchitectonic probabilities according to the SPM Anatomy Toolbox (Eickoff et al., 2005). The outermost right column indicates the maximal z-value of voxels within a cluster (with the mean z-value of all voxels within a cluster in parentheses). No significant differences were observed in the thalamus. Abbreviations: MCC: Middle Cingulate Cortex; PCC: Posterior Cingulate Cortex; ACC: Anterior Cingulate Cortex; IPL: Inferior Parietal Lobule; MTG: Middle Temporal Gyrus; SMG: Supramarginal Gyrus; STG: Superior Temporal Gyrus; SMG: Superior Medial Gyrus.

[a] The noted cluster covered 80% of the fastigial nucleus bilaterally and 12% of the left subiculum.

[b] The noted cluster covered 97% of the left fastigial nucleus.

increase in FC between the PCC and cerebellum is compensating the decrease of FC between BA39-BA19 and the cerebellum. Although technological factors that have limited the investigation of the cerebellum (Skouras et al., 2018) may have prevented the attribution of a well-established and specific functional role for the FC between the cerebellum and BA39-BA19, it is also plausible that this FC serves unspecific functions and that this is precisely why it can be compensated robustly without any noticeable cognitive or behavioral consequences.

4.3. Functional connectivity in the MCI due to AD group

As AD progresses into the MCI stage, characterized by hippocampal neurodegeneration (Gispert et al., 2015), the PCu can no longer capacitate compensatory support for hippocampal decoupling. This is evident from the functional decoupling of PCu/cuneus from PCC (Table 5) corroborating previous evidence of lower FC in the PCu during the MCI stage (Binnewijzend and Schoonheim, 2012) and supporting models of preclinical compensation and clinical degradation in the PCu (Jack et al., 2013b; Jacobs et al., 2013). In response, functional coupling of PCC with the insula, BA47, superior temporal gyrus and left temporal pole emerges as an unexpected tertiary compensatory mechanism (Fig. 4; Table 5).

During the MCI stage of AD, functional coupling of MCC with the cerebellum, the posterior part of BA32 and the left BA8 can account for the emergence of new cognitive strategies that MCI subjects employ in order to compensate memory and cognitive impairments and manage to cope with their daily activities. In particular, the observed subregion of the cerebellum supports executive function (Habas et al., 2009) and has been observed to interact with the hippocampus during sequence-based navigation (Iglói et al., 2015). The observed subregion of BA32 subserves working memory (Hill et al., 2014; Wager and Smith, 2003; Zhang et al., 2003), while BA8 appears to be involved in working memory (Babiloni et al., 2005) and processing related to uncertainty (Volz et al., 2004). Additional evidence suggests that BA8 is one of the main loci of autobiographical memory (Janata, 2009) and significantly more so in borderline personality disorder patients (Schnell et al., 2007), a population that also suffers from reduced hippocampal volume (Driessen et al., 2000) similarly to the MCI group due to AD (Gispert et al., 2015). Based on all evidence, it is plausible that the stronger coupling between MCC and cerebellum in the MCI group, represents an effort to counteract the uncertainty that results from loss of memory due to hippocampal atrophy, via increased processing in areas with uncompromised neural capacity, in order to maintain the ability to execute complete sequences of actions.

4.4. Functional connectivity in the dementia due to AD group

As expected, extensive and uncompensated functional decoupling is observed in the stage of dementia due to AD (Fig. 5; Table 6). The right BA21, involved in prosody processing (Ethofer et al., 2006; Hesling et al., 2005) and more importantly in memory integration (Backus et al., 2016), decouples from both the BA39-BA19 and MCC clusters. The BA39-BA19 and MCC clusters additionally decouple from the ACC and PCC respectively, exhibiting in this stage for the first time an anti-correlation pattern among ECM clusters. Moreover, the lingual gyrus decouples from ACC but increases FC with MCC and PCC, continuing the compensatory effort commenced during the preclinical stage.

The functional decoupling of the middle temporal gyrus, superior temporal gyrus and BA21 from both the BA39-BA19 and MCC (BA24) clusters, in combination with the decoupling of BA39-BA19 from an extensive medial frontal cluster that includes ACC, BA32, BA9, BA10 and BA11, remain uncompensated and appear to be underpinning the dysfunctional state of dementia due to AD. Indeed, BA21 and BA22 are involved in the crucial function of memory integration (Backus et al., 2016). Moreover, the observed frontal cluster engulfs the neural substrates of the self-memory system subserving episodic autobiographical memory, semantic autobiographical memory and memory of the conceptual self (Martinelli et al., 2013). The extensive functional decoupling of these areas with BA39-BA19 is illustrating the final collapsing of memory functions in dementia due to AD.

4.5. Relevance to contemporary theories

Our findings provide evidence of convergence between two complementary theoretical frameworks: a) the 'compensation-related utilization of neural circuits hypothesis' (CRUNCH; Reuter-Lorenz and Cappell, 2008) and b) the 'network-based degeneration' theory (Seeley et al., 2009). The integration of these two perspectives has been

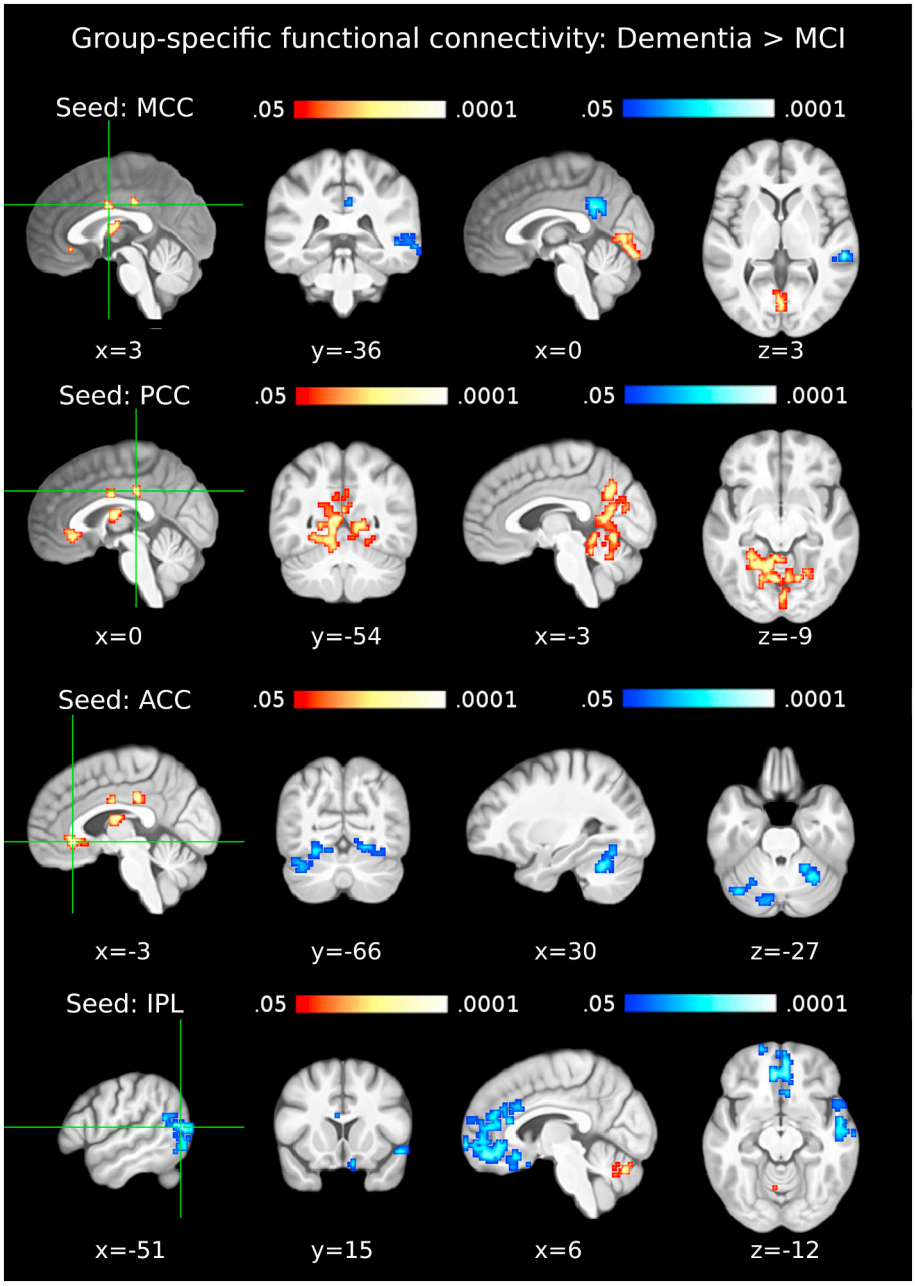

Fig. 5. Functional connectivity in the dementia due to AD group. The first column shows seed clusters derived by the data-driven ECM analysis. The results of the comparison of functional connectivity maps between dementia and MCI due to AD (Dementia > MCI) are shown in each row, separately for four seed regions (MCC: first row, PCC: second row, ACC: third row, IPL (BA39-BA19): fourth row). The remaining ECM cluster, in the thalamus, did not show functional connectivity differences between dementia and MCI groups. Increases are depicted in red and decreases in blue color; images are shown in neurological convention; all results are corrected for multiple comparisons ($P < 0.05$); coordinates refer to MNI space. (For interpretation of the references to color in this figure legend, the reader is referred to the web version of this article.)

suggested in a recent meta-analysis of functional network alterations in AD, proposing that in the preclinical stage, compensatory mechanisms arise in the form of increased functional connectivity to counteract connectivity loss in other regions, while in more advanced stages this compensatory mechanism breaks down as a result of increasing local and global neurodegenerative pathology (Jacobs et al., 2013). We provide voxel-wise maps that depict in unprecedented detail the progressive processes that have been proposed by these contemporary theories, while highlighting their relevance to cognitive functions. NIfTI images of our findings will be shared upon request, along with the scripted analysis pipeline, to facilitate replicable Open Science practices.

4.6. Limitations and future directions

We have adopted the most straightforward interpretation of considering decreases in EC and FC to be due to AD progression and spatially linked concurrent increases to correspond to compensatory mechanisms. Moreover, we assumed that functional decoupling between two brain regions represents functional degradation and can be compensated by concurrent coupling of either decoupled region with alternative ones. Two further implicit assumptions were that the cross-sectional p-tau/Aβ42 ratio is a valid marker of position along the AD continuum and that diagnostic categories are sequential and irreversible. Although our assumptions are largely supported in literature, by the current theoretical framework (Reuter-Lorenz and Cappell, 2008; Seeley et al., 2009; Barulli and Stern, 2013; Jacobs et al., 2013), by the corroborated meta-analyses discussed (Jacobs et al., 2013; Martinelli et al., 2013), as well by a complementary volumetric study of the same population (Gispert et al., 2015), it remains likely that the underlying mechanisms are of higher complexity. Moreover, due to directional testing, we observed a few findings that were neither expected nor entirely supported by the statistical framework employed, e.g. at the insula. We note these unexpected findings in the Supplementary Material, because many of them have plausible interpretations that may be useful for the formation of future experimental hypotheses. It will be

important for the main findings to be replicated and confirmed in longitudinal studies using larger samples, especially with regards to the preclinical group. Nevertheless, we believe that the patterns of voxel-wise connectomics revealed here can be informative for future diagnostic procedures and contribute valuable insights towards appreciating the distributed functional capacity of the human brain.

5. Conclusions

Preclinical functional decoupling occurs predominantly in AD-vulnerable regions (e.g. hippocampus, cerebellar lobule VI / Crus I, visual cortex, frontal pole) and each AD stage is characterized by distinct patterns of FC. Plausible mechanisms of functional compensation across the AD continuum, appear primarily in three specific forms of changes in connectivity as: a) increased EC of thalamus, BA24, BA31, BA23 and BA32 across the entire continuum; b) increased coupling of MCC with PCu and of PCC with cerebellar declive, BA18, lingual gyri and fusiform gyri in the preclinical stage and c) increased coupling of MCC with BA32, BA8 and cerebellar uvula and of PCC with inferio-anterior insula and BA47 in MCI.

Funding

This work has received funding from the European Union's Horizon 2020 research and innovation programme under the Marie Sklodowska-Curie action [grant agreement No 707730].

The research leading to these results has also received support from the Innovative Medicines Initiative Joint Undertaking under grant agreement n° 115568, resources of which are composed of financial contribution from the European Union's Seventh Framework Programme (FP7/2007-2013) and EFPIA companies' in-kind contribution. In addition, part of the data collection was financed by the Spanish Ministry of Economy and Competitiveness ISCIII which was co-funded by the European Regional Development Fund [grant number PI14/00282 (AL)]. JDG holds a "Ramón y Cajal" fellowship [RYC-2013-13054]. The present communication reflects the authors' view and neither IMI nor the European Union, EFPIA, or any Associated Partners are responsible for any use that may be made of the information contained herein.

Appendix A. Supplementary data

Supplementary data to this article can be found online at https://doi.org/10.1016/j.nicl.2019.101777.

References

Adriaanse, S.M., Wink, A.M., Tijms, B.M., Ossenkoppele, R., Verfaillie, S.C.J., Lammertsma, A.A., Boellaard, R., Scheltens, P., van Berckel, B.N.M., Barkhof, F., 2016. The association of glucose metabolism and eigenvector centrality in Alzheimer's disease. Brain Connectivity 6, 1–8.

Aggleton, J.P., Pralus, A., Nelson, A., Hornberger, M., 2016. Thalamic pathology and memory loss in early Alzheimer's disease: moving the focus from the medial temporal lobe to Papez circuit. Published online ahead of print.

Albada, V.S., Robinson, P.A., 2007. Transformation of arbitrary distributions to the normal distribution with application to EEG test–retest reliability. J. Neurosci. Methods 161, 205–211.

Andrews-Hanna, J.R., Reidler, J.S., Sepulcre, J., Poulin, R., Buckner, R.L., 2010. Functional-anatomic fractionation of the brain's default network. Neuron 65, 550–562.

Avants, B.B., Epstein, C.L., Grossman, M., Gee, J.C., 2008. Symmetric diffeomorphic image registration with cross-correlation: evaluating automated labeling of elderly and neurodegenerative brain. Med. Image Anal. 12, 26–41.

Avants, B.B., Tustison, N., Song, G., 2009. Advanced normalization tools (ANTS). Insight 2, 1–35.

Avants, B., Tustison, N., Song, G., Cook, P., Klein, A., Gee, J., 2010a. A reproducible evaluation of ANTs similarity metric performance in brain image registration. Neuroimage 54, 2033–2044.

Avants, B., Yushkevich, P., Pluta, J., Minkoff, D., Korczykowski, M., Detre, J., et al., 2010b. The optimal template effect in hippocampus studies of diseased populations. Neuroimage 49, 2457–2466.

Babiloni, C., Ferretti, A., Gratta, D.C., Carducci, F., 2005. Human cortical responses during one-bit delayed-response tasks: an fMRI study. Brain Res. Bull. 65, 383–390.

Bäckman, L., Jones, S., Berger, A.K., Laukka, E.J., 2005. Cognitive impairment in preclinical Alzheimer's disease: a meta-analysis. Neuropsychology 19, 520.

Backus, A.R., Schoffelen, J.M., Szebényi, S., Hanslmayr, S., 2016. Hippocampal-prefrontal theta oscillations support memory integration. Curr. Biol. 26, 450–457.

Barulli, D., Stern, Y., 2013. Efficiency, capacity, compensation, maintenance, plasticity: emerging concepts in cognitive reserve. Trends Cogn. Sci. 17, 502–509.

Binnewijzend, M., Schoonheim, M.M., 2012. Resting-state fMRI changes in Alzheimer's disease and mild cognitive impairment. Neurobiol. Aging 33, 2018–2028.

Binnewijzend, M., Adriaanse, S., Flier, W., Teunissen, C., Munck, J., Stam, C., et al., 2014. Brain network alterations in Alzheimer's disease measured by eigenvector centrality in fMRI are related to cognition and CSF biomarkers. Hum. Brain Mapp. 35, 2383–2393.

Bonacich, P., 1972. Technique for analyzing overlapping memberships. Sociol. Methodol. 4, 176–185.

Bonacich, P., 2007. Some unique properties of eigenvector centrality. Soc. Networks 29, 555–564.

Bonacich, P., Lloyd, P., 2004. Calculating status with negative relations. Soc. Networks 26 (4), 331–338.

Borgatti, S.P., 2005. Centrality and network flow. Soc. Networks 27, 55–71.

Brown, E.N., Behrmann, M., 2017. Controversy in statistical analysis of functional magnetic resonance imaging data. PNAS 114 (17), E3368–E3369.

Buckner, R., Sepulcre, J., Talukdar, T., Krienen, F., Liu, H., Hedden, T., et al., 2009. Cortical hubs revealed by intrinsic functional connectivity: mapping, assessment of stability, and relation to Alzheimer's disease. J. Neurosci. 29, 1860–1873.

Cavanna, A.E., Trimble, M.R., 2006. The precuneus: a review of its functional anatomy and behavioural correlates. Brain 129, 564–583.

Coupé, P., Yger, P., Prima, S., Hellier, P., Kervrann, C., Barillot, C., 2008. An optimized blockwise nonlocal means denoising filter for 3-D magnetic resonance images. Med. Imag. IEEE Trans. 27, 425–441.

Cox, R.W., Chen, G., Glen, D.R., Reynolds, R.C., Taylor, P.A., 2017. FMRI clustering in AFNI: false-positive rates redux. Brain Connectivity 7 (3), 152–171.

de Souza, L.C., Lamari, F., Belliard, S., Jardel, C., Houillier, C., De Paz, R., et al., 2011. Cerebrospinal fluid biomarkers in the differential diagnosis of Alzheimer's disease from other cortical dementias. J. Neurol. Neurosurg. Psychiatry 82, 240–246.

Dickerson, B.C., Bakkour, A., Salat, D.H., Feczko, E., Pacheco, J., et al., 2009. The cortical signature of Alzheimer's disease: regionally specific cortical thinning relates to symptom severity in very mild to mild AD dementia and is detectable in in asymptomatic amyloid-positive individuals. Cereb. Cortex 19, 497–510.

Driessen, M., Herrmann, J., Stahl, K., 2000. Magnetic resonance imaging volumes of the hippocampus and the amygdala in women with borderline personality disorder and early traumatization. Arch. Gen. Psychiatry 57, 1115–1122.

Dubois, B., Hampel, H., Feldman, H.H., Scheltens, P., Aisen, P., Andrieu, S., Bakardjian, H., Benali, H., Bertram, L., Blennow, K., et al., 2016. Preclinical Alzheimer's disease: definition, natural history, and diagnostic criteria. Alzheimer's Dementia 12, 292–323.

Eickhoff, S., Stephan, K., Mohlberg, H., Grefkes, C., Fink, G., Amunts, K., Zilles, K.., 2005. A new SPM toolbox for combining probabilistic cytoarchitectonic maps and functional imaging data. NeuroImage 25, 1325–1335.

Elman, J.A., Madison, C.M., Baker, S.L., Vogel, J.W., Marks, S.M., Crowley, S., et al., 2016. Effects of beta-amyloid on resting state functional connectivity within and between networks reflect known patterns of regional vulnerability. Cereb. Cortex 26, 695–707.

Ethofer, T., Anders, S., Erb, M., Herbert, C., Wiethoff, S., 2006. Cerebral pathways in processing of affective prosody: a dynamic causal modeling study. Neuroimage 30, 580–587.

Fagan, A.M., Roe, C.M., Xiong, C., 2007. Cerebrospinal fluid tau/β-amyloid42 ratio as a prediction of cognitive decline in nondemented older adults. Arch. Neurol. 64, 343–349.

Fisher, R.A., 1915. Frequency distribution of the values of the correlation coefficient in samples of an indefinitely large population. Biometrika 10 (4), 507–521.

Fisher, R.A., 1921. On the 'probable error' of a coefficient of correlation deduced from a small sample. Metron. 1, 3–32.

Fonov, V., Evans, A.C., Botteron, K., Almli, R.C., McKinstry, R.C., Collins, L.D., 2011. Unbiased average age-appropriate atlases for pediatric studies. NeuroImage 54, 313–327.

Fortea, J., Sala-Llonch, R., Bartrés-Faz, D., Lladó, A., 2011. Cognitively preserved subjects with transitional cerebrospinal fluid ss-amyloid 1-42 values have thicker cortex in Alzheimer's disease vulnerable areas. Biol. Psychiatry 70, 183–190.

Gallichan, D., Scholz, J., Bartsch, A., Behrens, T., Robson, M., Miller, K., 2010. Addressing a systematic vibration artifact in diffusion-weighted MRI. Hum. Brain Mapp. 31, 193–202.

Ghaem, O., Mellet, E., Crivello, F., Tzourio, N., Mazoyer, B., 1997. Mental navigation along memorized routes activates the hippocampus, precuneus, and insula. Neuroreport 8, 739–744.

Gilbert SJ, Dumontheil I, Simons JS, Frith CD, Burgess PW (2007): Comment on "Wandering minds: the default network and stimulus-independent thought." Science 317:43.

Gispert, J.D., Rami, L., Sánchez-Benavides, G., Falcon, C., Tucholka, A., Rojas, S., et al., 2015. Nonlinear cerebral atrophy patterns across the Alzheimer's disease continuum: impact of APOE4 genotype. Neurobiol. Aging 36, 2687–2701.

Grober, E., Buschke, H., 1987. Genuine memory deficits in dementia. Dev. Neuropsychol. 3, 13–36.

Grober, E., Ocepek-Welikson, K., Teresi, J.A., 2009. The free and cued selective reminding

test: evidence of psychometric adequacy. Psychol. Sci. Q. 51, 266–282.
Guo, C.C., Tan, R., Hodges, J.R., Hu, X., Sami, S., 2016. Network-selective vulnerability of the human cerebellum to Alzheimer's disease and frontotemporal dementia. Brain 139, 1527–1538.
Gusnard, D.A., Raichle, M.E., 2001. Searching for a baseline: functional imaging and the resting human brain. Nat. Rev. Neurosci. 2, 685–694.
Habas, C., Kamdar, N., Nguyen, D., Prater, K., 2009. Distinct cerebellar contributions to intrinsic connectivity networks. J. Neurosci. 29, 8586–8594.
Hesling, I., Clément, S., Bordessoules, M., Allard, M., 2005. Cerebral mechanisms of prosodic integration: evidence from connected speech. Neuroimage 24, 937–947.
Hill, A.C., Laird, A.R., Robinson, J.L., 2014. Gender differences in working memory networks: a BrainMap meta-analysis. Biol. Psychol. 102, 18–29.
Iglói, K., Doeller, C.F., Paradis, A.-L., Benchenane, K., Berthoz, A., Burgess, N., et al., 2015. Interaction between hippocampus and cerebellum crus I in sequence-based but not place-based navigation. Cereb. Cortex 25, 4146–4154.
Jack, C., Knopman, D., Jagust, W., Petersen, R., Weiner, M., Aisen, P., et al., 2013a. Tracking pathophysiological processes in Alzheimer's disease: an updated hypothetical model of dynamic biomarkers. Lancet Neurol. 12, 207–216.
Jack, C., Wiste, H., Weigand, S., Knopman, D., Lowe, V., Vemuri, P., et al., 2013b. Amyloid-first and neurodegeneration-first profiles characterize incident amyloid PET positivity. Neurology 81, 1732–1740.
Jack, C.R., Bennett, D.A., Blennow, K., Carrillo, M.C., Dunn, B., Haeberlein, S.B., et al., 2018. NIA-AA Research Framework: Toward a biological definition of Alzheimer's disease. Alzheimers Dement. 14, 535–562.
Jacobs, H., Radua, J., Lückmann, H.C., 2013. Meta-analysis of functional network alterations in Alzheimer's disease: toward a network biomarker. Neurosci. Biobehav. Rev. 37, 753–765.
Janata, P., 2009. The neural architecture of music-evoked autobiographical memories. Cereb. Cortex 19, 2579–2594.
Koelsch, S., Skouras, S., 2014. Functional centrality of amygdala, striatum and hypothalamus in a “small-world” network underlying joy: An fMRI study with music. Hum. Brain Mapp. 35, 3485–3498.
Langville, A., Meyer, C., 2006. The Mathematics of Google's PageRank. In: Google's PageRank and Beyond: The Science of Search Engine Rankings. Princeton University Press, Princeton and Oxford, pp. 31–46.
Leal, S.L., Landau, S.M., Bell, R.K., Jagust, W.J., 2017. Hippocampal activation is associated with longitudinal amyloid accumulation and cognitive decline. eLife 6, e22978.
Lemieux, L., Salek-Haddadi, A., Lund, T.E., Laufs, H., 2007. Modelling large motion events in fMRI studies of patients with epilepsy. Magn. Reson. Imaging 25, 894–901.
Li, G., Sokal, I., Quinn, J.F., Leverenz, J.B., Brodey, M., Schellenberg, G.D., Kaye, J.A., Raskind, M.A., Zhang, J., Peskind, E.R., et al., 2007. CSF tau/Aβ42 ratio for increased risk of mild cognitive impairment a follow-up study. Neurology 69, 631–639.
Lohmann, G., Müller, K., Bosch, V., Mentzel, H., Hessler, S., 2000. LIPSIA-Leipzig Image Processing and Statistical Inference Algorithms.
Lohmann, G., Neumann, J., Müller, K., 2008. The Multiple Comparison Problem in Fmri - a New Method Based on Anatomical Priors. (Proceedings of the First Workshop on Analysis of Functional Medical Images).
Lohmann, G., Margulies, D.S., Horstmann, A., Pleger, B., Lepsien, J., Goldhahn, D., et al., 2010. Eigenvector centrality mapping for analyzing connectivity patterns in fMRI data of the human brain. PLoS One 5, e10232.
Maddalena, A., Papassotiropoulos, A., Müller-Tillmanns, B., Jung, H.H., Hegi, T., Nitsch, R.M., Hock, C., 2003. Biochemical diagnosis of Alzheimer disease by measuring the cerebrospinal fluid ratio of phosphorylated tau protein to β-amyloid peptide42. Arch. Neurol. 60, 1202–1206.
Martinelli, P., Sperduti, M., Piolino, P., 2013. Neural substrates of the self-memory system: new insights from a meta-analysis. Hum. Brain Mapp. 34, 1515–1529.
Molinuevo, J., Gispert, J., Dubois, B., Heneka, M., Lleo, A., Engelborghs, S., et al., 2013. The AD-CSF-index discriminates Alzheimer's disease patients from healthy controls: a validation study. J. Alzheimers Dis. 36, 67–77.
Palmqvist, S., Schöll, M., Strandberg, O., Mattsson, N., Stomrud, E., Zetterberg, H., Blennow, K., Landau, S., Jagust, W., Hansson, O., 2017. Earliest accumulation of β-amyloid occurs within the default-mode network and concurrently affects brain connectivity. Nat. Commun. 8, 1214.
Pihlajamäki, M., Sperling, R.A., 2008. fMRI: use in early Alzheimer's disease and in clinical trials. Future Neurol. 3, 409–421.
Poline, J.B., Worsley, K.J., Evans, A.C., Friston, K.J., 1997. Combining spatial extent and peak intensity to test for activations in functional imaging. Neuroimage 5 (2), 83–96.
Raichle, M.E., MacLeod, A.M., Snyder, A.Z., Powers, W.J., Gusnard, D., et al., 2001. A default mode of brain function. PNAS 98, 676–682.
Rami, L., Molinuevo, J.L., Sanchez-Valle, R., 2007. Screening for amnestic mild cognitive impairment and early Alzheimer's disease with M@ T (memory alteration test) in the primary care population. Int. J. Geriatric Psychiatry 22, 294–304.
Reuter-Lorenz, P.A., Cappell, K.A., 2008. Neurocognitive aging and the compensation hypothesis. Curr. Dir. Psychol. Sci. 17 (3), 177–182.
Sadananthan, S.A., Zheng, W., Chee, M.W., Zagorodnov, V., 2010. Skull stripping using graph cuts. NeuroImage 49 (1), 225–239.
Schnell, K., Dietrich, T., Schnitker, R., Daumann, J., 2007. Processing of autobiographical memory retrieval cues in borderline personality disorder. J. Affect. Disord. 97, 253–259.
Schoonheim, M.M., Geurts, J.J.G., Wiebenga, O.T., De Munck, J.C., Polman, C.H., Stam, C.J., Barkhof, F., Wink, A.M., 2014. Changes in functional network centrality underlie cognitive dysfunction and physical disability in multiple sclerosis. Mult. Scler. J. 20, 1058–1065.
Seeley, W.W., Crawford, R.K., Zhou, J., Miller, B.L., Greicius, M.D., 2009. Neurodegenerative diseases target large-scale human brain networks. Neuron 62, 42–52.
Sheline, Y., Raichle, M., 2013. Resting state functional connectivity in preclinical Alzheimer's disease. Biol. Psychiatry 74, 340–347.
Shulman, G.L., Fiez, J.A., Corbetta, M., Buckner, R.L., Miezen, F.M., Raichle, M.E., et al., 1997. Common blood flow changes across visual tasks, II: decreases in cerebral cortex. J. Cogn. Neurosci. 9, 648–663.
Skouras, S., Gray, M., Critchley, H., Koelsch, S., 2014. Superficial amygdala and hippocampal activity during affective music listening at 3 T but not 1.5 T fMRI. NeuroImage 101, 364–369. https://doi.org/10.1016/j.neuroimage.2014.07.007.
Skouras, S., Gispert, J.D., Molinuevo, J.L., 2018. The crus exhibits stronger functional connectivity with executive network nodes than with the default mode network. Brain 141, e24.
Smith, S.M., Nichols, T.E., 2009. Threshold-free cluster enhancement: addressing problems of smoothing, threshold dependence and localisation in cluster inference. Neuroimage 44 (1), 83–98.
Söderlund, H., Moscovitch, M., Kumar, N., Mandic, M., 2012. As time goes by: hippocampal connectivity changes with remoteness of autobiographical memory retrieval. Hippocampus 22, 670–679.
Sperling, R.A., Aisen, P.S., Beckett, L.A., Bennett, D.A., Craft, S., Fagan, A.M., Iwatsubo, T., Jack, C.R., Kaye, J., Montine, T.J., Park, D.C., 2011. Toward defining the preclinical stages of Alzheimer's disease: recommendations from the National Institute on Aging-Alzheimer's Association workgroups on diagnostic guidelines for Alzheimer's disease. Alzheimers Dement. 7, 280–292.
Spreng, R.N., Stevens, W.D., Chamberlain, J.P., Gilmore, A.W., Schacter, D.L., 2010. Default network activity, coupled with the frontoparietal control network, supports goal-directed cognition. Neuroimage 53 (1), 303–317.
Strassnig, M., Ganguli, M., 2005. About a peculiar disease of the cerebral cortex: Alzheimer's original case revisited. Psychiatry (Edgmont) 2 (9), 30–33.
Teipel, S., Drzezga, A., Grothe, M.J., Barthel, H., 2015. Multimodal imaging in Alzheimer's disease: validity and usefulness for early detection. Lancet Neurol. 14, 1037–1053.
Tustison, N.J., Avants, B.B., 2013. Explicit B-spline regularization in diffeomorphic image registration. Front. Neuroinform. 7, 39.
Tustison, N., Avants, B., Cook, P., Zheng, Y., Egan, A., Yushkevich, P., et al., 2010. N4ITK: improved N3 bias correction. IEEE Ttans. Med. Imaging 29, 1310–1320.
Tustison, N.J., Avants, B.B., Cook, P.A., 2013. The ANTs Cortical Thickness Processing Pipeline. (SPIE Medical Imaging. International Society for Optics and Photonics).
Volz, K.G., Schubotz, R.I., von Cramon, D.Y., 2004. Why am I unsure? Internal and external attributions of uncertainty dissociated by fMRI. Neuroimage 21, 848–857.
Wager, T.D., Smith, E.E., 2003. Neuroimaging studies of working memory. Cogn. Affect. Behav. Neurosci. 3, 255–274.
Wang, L., Zang, Y., He, Y., Liang, M., Zhang, X., Tian, L., et al., 2006. Changes in hippocampal connectivity in the early stages of Alzheimer's disease: evidence from resting state fMRI. Neuroimage 31, 496–504.
Wesson, J., Luchins, J., 1992. An empirical evaluation of the global deterioration scale for staging Alzheimer's disease. Am. J. Psychiatry 149, 190–194.
Wink, A.M., de Munck, J.C., van der Werf, Y.D., van den Heuvel, O.A., Barkhof, F., 2012. Fast eigenvector centrality mapping of voxel-wise connectivity in functional magnetic resonance imaging: implementation, validation, and interpretation. Brain Connectivity 2 (5), 265–274.
Zhang, J.X., Leung, H.C., Johnson, M.K., 2003. Frontal activations associated with accessing and evaluating information in working memory: an fMRI study. Neuroimage 20, 1531–1539.